Submitted to the 30th International Conference on High-Energy Physics ICHEP2000,
Osaka, Japan, July 2000

Measurements of 2-Jet and 3-Jet Cross Sections at High Transverse Momentum in Photoproduction

H1 Collaboration

Abstract

Single differential 2-jet and 3-jet cross sections as a function of jet transverse momentum and invariant mass are measured in photoproduction using the H1 detector at HERA. The data sample comprises all available e^+p data collected from 1994-97. Jets are found using the longitudinal boost-invariant K_T algorithm run in the laboratory frame with a minimum transverse momentum of the highest transverse momentum jet of greater than $25\ \mathrm{GeV}$. When the cross sections for two and three jet production are compared with QCD predictions, no significant deviations from expectation are found.

Abstract: 977/978
Parallel session: 3,11
Plenary talk: 11,7b

1 Introduction and Motivation

At HERA high transverse momentum jets are preferentially produced in photoproduction where the photon virtuality, $Q^2 \approx 0\ \mathrm{GeV}^2$. In this paper single differential photoproduction 2-jet and 3-jet ep cross sections in jet transverse momentum P_T^{jet} up to $\sim 75\mathrm{GeV}$ and invariant mass up to $\sim 180\mathrm{GeV}$ are presented. These jet cross sections are sensitive primarily to the dynamics of the hard partonic scatter, allowing the validity of Quantum Chromodynamics (QCD) to be tested up to the highest transverse momenta and masses available at HERA. The understanding of QCD jet production is essential if the sensitivity to hadronic decays of massive particles is to be exploited.

A data sample requiring at least two hard jets of which one must have transverse momentum greater than $25\ \mathrm{GeV}$ is defined. A subsample, requiring a third hard jet, is then constructed. From these samples differential 2-jet and 3-jet ep cross sections in jet transverse momentum and jet invariant mass are evaluated.

The paper is organized as follows. In section 2 the H1 detector is presented while Section 3 reviews the theoretical models. The jet algorithm used and the phase space considered in the analysis are defined in section 4. Section 5 details the analysis method. A discussion of the cross section measurements is presented in section 6. The final section provides a summary of the results and their interpretation. A full description of the analysis may be found in [1].

2 The H1 Detector

The H1 detector is described in detail in [2]. Only those components relevant to the analysis are described here. The Liquid Argon (LAC) [3] and SpaCal [4] calorimeters are used to trigger events, reconstruct the hadronic energy of the final state and anti-tag positrons. The central tracking detector (CTD) is used to reconstruct the interaction vertex and to supplement the measurement of hadronic energy flow. A coordinate system in which the nominal interaction point is at the origin and the incident proton beam defines the $+z$ direction is used.

The LAC covers the polar angle range $4^\circ < \theta < 154^\circ$ with full azimuthal acceptance. It consists of an electromagnetic section and a hadronic section. The total depth varies between 4.5 and 8 hadronic interaction lengths. The angular region $153^\circ < \theta < 177.8^\circ$ is covered by the SpaCal, a lead/scintillating-fibre calorimeter. It also contains an electromagnetic and a hadronic section. The hadronic energy scale of the LAC is known to 4% and of the SpaCal to 7%.

The CTD consists of two concentric cylindrical drift chambers, coaxial with the beam-line, with a polar angle coverage of $15^\circ < \theta < 165^\circ$. The entire CTD is immersed in a 1.15 T magnetic field. The luminosity determination is based on measurement of the $ep \to ep\gamma$ Bethe-Heitler process, where the positron and photon are detected in crystal Cherenkov calorimeters located downstream of the interaction point.

Model	α_s name	$\Lambda^{[4]}_{QCD}$ (MeV)	Proton PDF	γ PDF	P_t^{min} (GeV)	MI Scheme	P_T^{MI} (GeV)
PYTHIA	1-loop	200	GRV-LO	GRV-LO	6	MSTP(82)=1	1.2
HERWIG	2-loop ($\overline{MS}$)	291	GRV-LO	GRV-LO	6	20% SUE	-

Table 1: Description of event generators used to simulate photoproduction processes.

3 Theoretical Models and Simulations

In this paper QCD-inspired Monte Carlo event generators are used to unfold the data and, along with next to leading order (NLO) QCD calculations, are compared to the corrected data cross sections. A brief description of the generators and calculations used for these purposes are described below.

To simulate the direct and resolved QCD photoproduction of jets the PYTHIA 5.7 [5] and HERWIG 5.9 [6] event generators are used. Both programs contain the Born level QCD hard scattering matrix elements, regulated by a minimum cutoff, P_T^{min} . Leading logarithmic parton showers simulate higher order QCD radiation. GRV-LO [7] parton distribution functions (PDFs) for the proton and photon are applied. The Lund String model is used by PYTHIA to hadronize the outgoing partons, while HERWIG uses the Cluster Hadronization approach. Multiple interactions between the proton and resolved photon are dealt with in PYTHIA by extending the perturbative parton-parton scattering below $\hat{P}_T$, the transverse momentum of the main partonic scatter, to a new limit, P_T^{MI} . In HERWIG (in order to model the multiple interactions), 20$\%$ of events were simulated with the proton and resolved photon remnants interacting, producing soft particles. Table 1 summarizes the major parameters used in these two event generators. The EPVEC [8] program is used to model the contribution to the cross sections arising from real W production. A full detector simulation [9] is applied to all Monte Carlo events.

The JetViP [10] program, in which hard scattering matrix elements up to $\mathcal{O}(\alpha_s^3)$ are implemented, is also used to compare QCD predictions to the data. The VEGAS [11] package is used to perform the integration over the allowed phase space with five iterations to ensure stability. Divergences in the real and virtual corrections are handled by JetViP using the phase-space slicing approach. In calculating NLO 2-jet cross sections, 2-loop α_s with 5 flavours is used in the $\overline{MS}$ scheme and GRV-HO [7] PDFs chosen for the proton and photon, whilst for the (LO) 3-jet cross sections, 1-loop α_s with 5 flavours and GRV-LO PDFs were used. In all cases, Λ_{QCD} is taken from the proton PDF.

For estimating the Neutral Current Deep Inelastic Scattering (NC DIS) background, events with $Q^2 > 4\ \mathrm{GeV}^2$ were generated using RAPGAP 2.3 [12] with CTEQ4M [13] parameterizations for the proton (a structureless photon is assumed) and parton showering.

4 Jet Selection

The longitudinally boost-invariant K_T algorithm as proposed in [14] is used in this analysis to define jets. This algorithm avoids the ambiguities that occur in cone-type algorithms [15].

The algorithm is implemented using the KTCLUS [16] package and run in the inclusive mode. Details of the implementation of this algorithm can be found in [17]. The P_T -weighted scheme has been used throughout this analysis:

$$E_T^{jet} = \sum_i E_{T,i}, \qquad \eta^{jet} = \frac{\sum_i E_{T,i}\ \eta_i}{\sum_i E_{T,i}}, \qquad \phi^{jet} = \frac{\sum_i E_{T,i}\ \phi_i}{\sum_i E_{T,i}}, \tag{1}$$

where the index, i runs over all final state objects. Since the jets are defined as massless, the rapidity and pseudorapidity of the jets are equivalent, as are the transverse momentum, P_T^{jet} and transverse energy, E_T^{jet} .

Cuts on jet transverse momentum are made such that $P_T^{jet1} > 25$ GeV, $P_T^{jet2} > 15$ GeV and for the 3-jet sample, $P_T^{jet3} > 10$ GeV. The pseudorapidity of each jet, η^{jet} is restricted to $-0.5 < \eta^{jet} < 2.5$. All jets are then well contained in the LAC. Asymmetric cuts on the P_T^{jet} of the top two jets are made to avoid NLO uncertainties due to infrared-sensitive regions of phase space. The measured kinematic region is restricted to $y < 0.9$ and $Q^2 < 4\mathrm{GeV}^2$.

5 Cross Section Measurement Procedure

5.1 Event Selection

The data sample was collected with the H1 detector from 1994-97, when 820 GeV protons collided with 27.6 GeV positrons, resulting in a centre-of-mass energy of 300 GeV. The integrated luminosity obtained is 35.7 pb^{-1}. Energy deposits in the calorimeters and tracks in the CTD were combined to reconstruct the hadronic energy of events [18]. The z coordinate of the event vertex, reconstructed from hit pattens in the CTD, is limited to -36 $< z_{vertex} <$ 34 cm. A cut on the missing transverse momentum $P_{T,miss} <$ 20 GeV is imposed to remove Charged Current and non-ep events. Jet selections as described in section 4 are applied. The measured jet energies are calibrated to their true energies using a large sample of single jet NC DIS events. In these events the jet momentum may be precisely estimated from kinematic constrains [1].

The only significant background in the di-jet sample arises from NC DIS events. These are suppressed by removing events with a electron identified in the LAC or SpaCal with energy above 5 GeV and by requiring $y < 0.9$, with y reconstructed using hadronic variables [19]. Further cuts detailed in [1] reduce the contamination from NC DIS interactions to less than 4% in all bins.

Kinematic and jet distributions are well described by the Monte Carlo predictions.

5.2 Correction of the Data for Detector Effects

The data cross sections are obtained from the measured event rates by correcting for acceptance losses and inefficiencies bin-by-bin, using the cross-section weighted sum of events generated by PYTHIA and EPVEC. The background from NC DIS processes is estimated using RAPGAP and is subtracted on a statistical basis. The bin purity, defined as the number of events generated and reconstructed in a bin divided by the number reconstructed in the bin, is greater than 35% for each bin. The ratio of bin contents before and after detector simulation is close to one. Bin centre corrections, radiative corrections and hadronization corrections are not applied.

5.3 Systematic Uncertainties

The systematic error on the measurement arises from the following sources:

- A 4 % uncertainty on the jet energy scale including a 2 % uncertainty that is correlated bin to bin. The jet energy scale uncertainty results in an error of 15–20 % on the cross sections.
- The uncertainty in the acceptance correction was estimated by taking the difference between the corrections obtained from HERWIG and PYTHIA. The resulting error on the cross sections is $\sim 10\%$.
- The uncertainty in the trigger efficiency results in a error of $\sim 4\%$ on the cross section.
- The uncertainty on the background from DIS events is evaluated by varying the Monte Carlo estimate by $\pm 100\%$. The resulting error on the cross sections is $\sim 1\%$.
- The uncertainty in the integrated luminosity results in an overall normalisation error of 1.5% on the cross section.

All systematic errors are added in quadrature.

6 Results

Cross sections for the 2-jet sample as functions of the transverse momentum of the leading jet and the average of the two leading jets are shown in figure 1. Cross sections for the 3-jet sample as functions of the transverse momentum of the third highest jet, the invariant mass of the two leading jets M^{12} and of all three jets M^{123} are shown in figure 2. In the measured ranges the cross sections fall by three orders of magnitude. The total uncertainty, evaluated by adding systematic and statistical errors in quadrature, is typically 15% on the 2-jet cross sections and 20% on the 3-jet cross sections.

The shape of the data are well described by the implementations of PYTHIA 5.7 and HERWIG 5.9. Hadronization corrections are studied with PYTHIA and HERWIG by comparing cross sections before and after hadronization of the outgoing partons (after parton showering). The correction is $\sim 10\%$ or lower in all bins and is not applied to the data, nor to any of the QCD models. The cross sections are also compare to QCD calculations as implemented in the JetViP program. The calculations agree well in shape and normalisation with the data.

The kinematic configuration of massive particle decay would correspond in the 3-jet sample to the case where all three jets have large transverse momenta and are well separated from each other such that invariant masses of jet pairs are large. While no significant deviation is seen in figure 2 it is noted that the QCD prediction yields a considerable number of events also at large P_T^{jet} and invariant mass in the inclusive distributions presented here. In the highest bin of the invariant mass of the top three jets, the EPVEC generation of W production ($ep \to eqW$, $W \to qq$) accounts for 7% of the cross section prediction.

7 Conclusions

Photoproduction of jets with high transverse momentum is investigated. Cross sections are measured for two or more jets and three or more jets as a function of transverse momentum up to $75\mathrm{GeV}$ and as a function of invariant mass up to $180\mathrm{GeV}$. The measured cross sections are compatible within errors with QCD predictions for photoproduction processes based on Monte Carlo event generator models and NLO QCD calculations.

Acknowledgements

We are grateful to the HERA machine group whose outstanding efforts have made and continue to make this experiment possible. We thank the engineers and technicians for their work in constructing and now maintaining the H1 detector, our funding agencies for financial support, the DESY technical staff for continual assistance, and the DESY directorate for the hospitality which they extend to the non-DESY members of the collaboration. We wish to thank B. Pötter and M. Seymour for many helpful discussions.

References

[1] Paul Bate; PhD thesis, Univ. of Manchester, England : "High Transverse Momentum 2-Jet and 3-Jet Cross Section Measurements in Photoproduction".

[2] H1 Collaboration, I. Abt et al., Nucl. Instr. and Meth. **A386** (1997) 310 and 348.

[3] H1 Calorimeter Group, B. Andrieu et al., Nucl. Instr. and Meth. **A336** (1993) 460.

[4] H1 SpaCal Group, R. D. Appuhn et al., Nucl. Instr. and Meth. **A386** (1997) 397.

[5] T. Sjostrand, CERN-TH-6488 (1992), Comput. Phys. Commun. **82** (1994) 74.

[6] G. Marchesini et al., Comp. Phys. Comm. **67** (1992) 465.

[7] M. Glück, E. Reya and A. Vogt, Phys. Rev. **D46** (1992) 1973.

[8] U. Baur, J.A.M. Vermaseren and D. Zeppenfeld, Nucl. Phys. **B375** (1992) 3.

[9] R. Brun et al., GEANT3 User's Guide, CERN-DD/EE-84-1 (1987).

[10] B. Potter, Comput. Phys. Commun. **119** (1999) 45.

[11] G.P. Lepage, J. Comp. Phys. **27** (1978) 192.

[12] H. Jung, Comp. Phys. Comm. **86** (1995) 147.

[13] H. L. Lai et al., Phys. Rev. **D55** (1997), 1280.

[14] S.D. Ellis and D.E. Soper, Phys. Rev. **D48** (1993) 3160.

[15] M.H. Seymour, in: Les Rencontres de la Vallée d'Aoste, La Thuile, France (1997) and Nucl. Phys. **B513** (1998) 269.

[16] S. Catani, Yu.L. Dokshitzer, M.H. Seymour and B.R. Webber, Nucl. Phys. **B406** (1993) 187.

[17] H1 Collab., C. Adloff et al., Nucl. Phys. **B545** (1999) 3.

[18] H1 Collab., C. Adloff et al., Z. Phys. **C74** (1997) 221.

[19] A. Blondel and F. Jacquet, Proceedings of the Study of an ep Facility for Europe ed. U. Amaldi, DESY 79/48 (1979) 391.

[20] L.A. del Pozo, PhD Thesis University of Cambridge, Cambridge, England (1993) RALT-002.

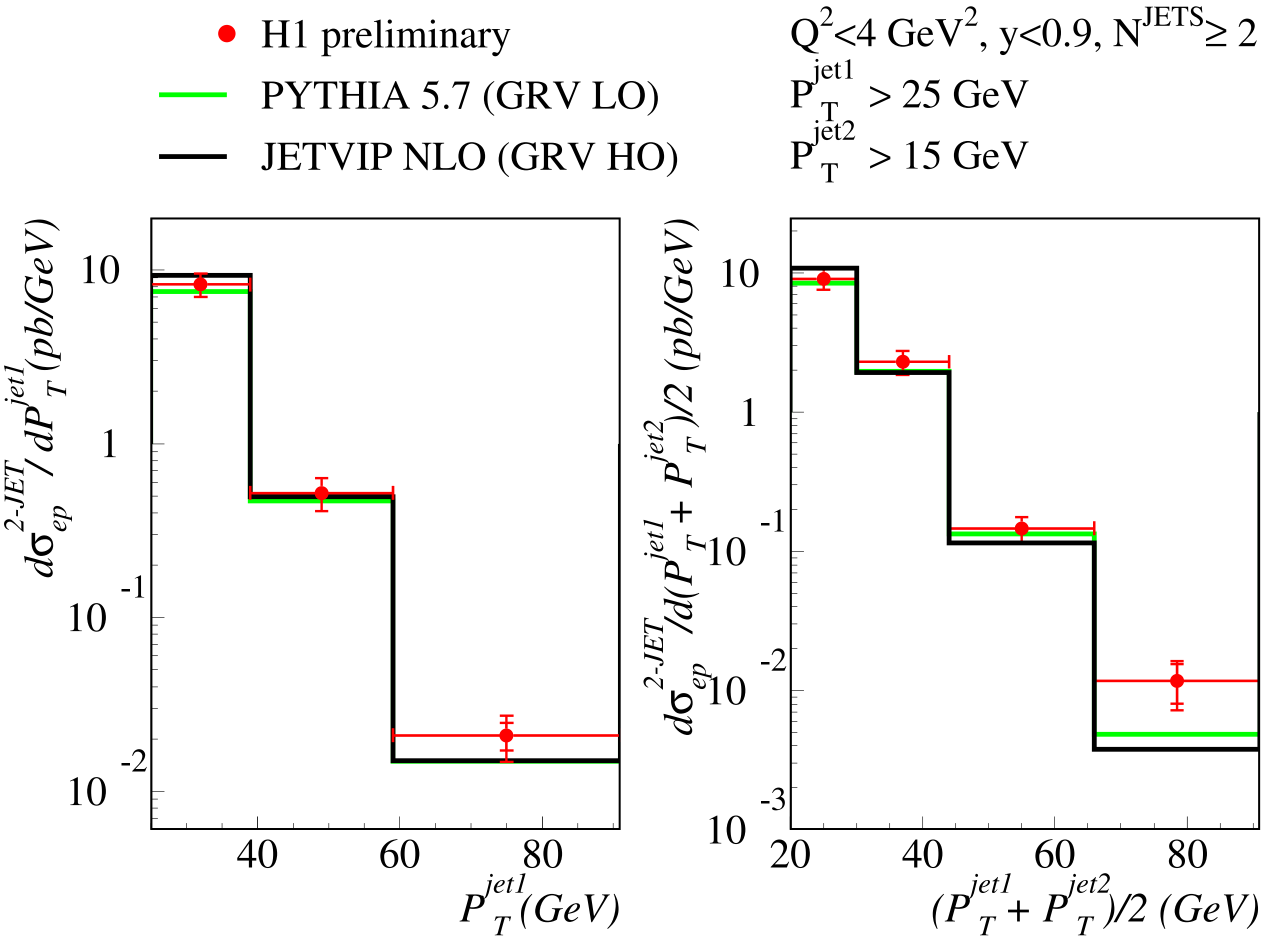

Figure 1: Hadronic cross sections for 2-jet production as function of the leading jet transverse momentum, P_T^{Jet1} (left) and the average transverse momentum of the top two jets, $(P_T^{Jet1} + P_T^{Jet2})/2$ (right) . The inner error bars denotes the statistical, the outer error bars the quadratic sum of all statistical and systematic errors of the data. The predictions given by the PYTHIA 5.7 using GRV-LO structure functions for the proton and photon are shown, as are the NLO parton cross sections implemented with the JetViP numerical integration program using GRV-HO structure functions respectively.

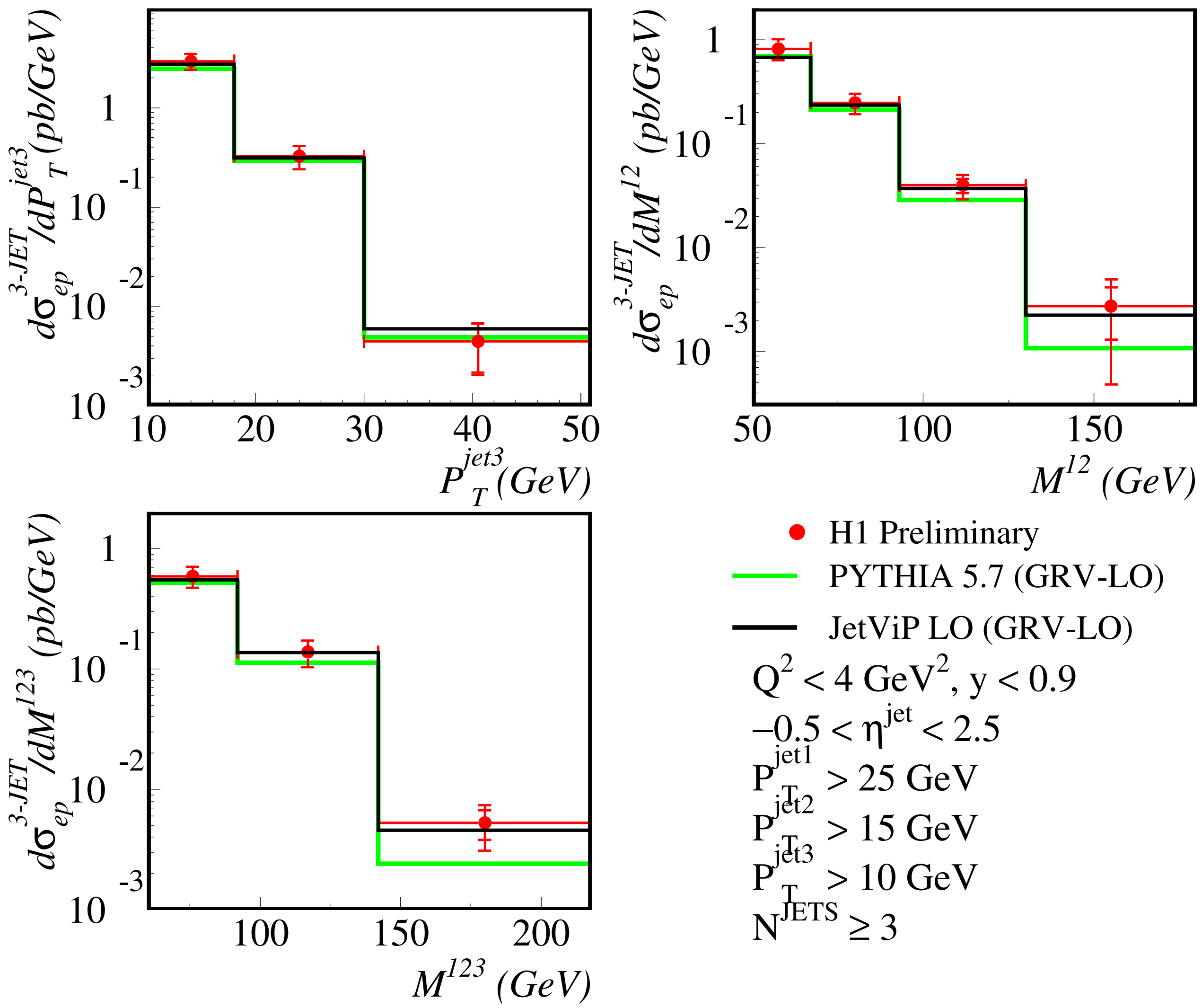

Figure 2: Hadronic cross sections for 3-jet production as function of the jet transverse momentum of the third highest jet P_T^{Jet3} (top left); as function of the invariant mass of the two leading jets M^{12} (top right) and as function of all three jets M^{123} (lower left). The inner error bars denotes the statistical, the outer error bars the quadratic sum of all statistical and systematic errors of the data. The predictions given by the PYTHIA 5.7, using GRV-LO structure functions for the proton and photon are shown, as is the LO parton cross sections implemented with the JetViP numerical integration program using GRV-LO structure functions.